# Effect of Undulations on Surface Tension in Simulated Bilayers

**S. J. Marrink* and A. E. Mark**

*Department of Biophysical Chemistry, University of Groningen, Nijenborgh 4, 9747 AG Groningen, The Netherlands*

*Received: January 26, 2001; In Final Form: April 19, 2001*

To understand the effect of the finite size of simulation cells on the equilibrium properties of bilayers, an extensive series of glycerolmonoolein bilayer molecular dynamics simulations in which the surface area and system size were systematically changed have been conducted. Systems ranging from 200 to 1800 lipids were simulated, covering length scales up to 20 nm. The dependence of the surface tension on the area per lipid is shown, although long simulation times were needed (up to 40 ns) to obtain reliable estimates. As the size of simulated patches increases, long wavelength undulatory modes appear with a concomitant increase in the area compressibility due to coupling of undulation modes to area fluctuations. Both the undulatory intensities and the peristaltic intensities of the bilayer fluctuations can be fitted in the long wavelength limit to continuum model predictions. The effect of system size on surface tension appears to depend on the stress conditions.

## I. Introduction

On a microscopic scale, molecular dynamics (MD) simulations have provided a lot of insight into the structure and dynamics of lipids and lipid−peptide or lipid−protein interactions (e.g., see refs 1−3). Because of increased computer power and advances in simulation algorithms MD simulations of lipid bilayers are now moving into the mesoscopic regime. In this regime, collective phenomena can be observed that occur on length scales larger than ∼10 nm and time scales of the order of 10 ns. The appearance of spontaneous undulations is an example of such a collective effect as it was recently observed in MD simulations by Lindahl and Edholm[4] who obtained accurate estimates of mesoscopic properties such as the bilayer bending constant.

Such simulations are important to be able to understand at which point the microscopic behavior turns into mesoscopic behavior and to estimate the effect of finite size and finite simulation time employed in MD simulations of bilayer systems. The recent debate in the literature concerning whether small scale systems have an equilibrium area per lipid which is too small due to suppressed undulations (i.e., refs 5 and 6) illustrates the importance of understanding finite size effects. Starting as a mainly theoretical discussion, extended simulations now make it possible to directly study these finite size effects. Nevertheless, the item is still unresolved. Feller and Pastor[7] claimed that a finite surface tension is required in a realistic simulation of a DPPC membrane to compensate for the suppressed undulations, Tieleman and Berendsen[8] did not, however, find a significant dependence of surface tension on surface area at all. In a further complication, Lindahl and Edholm[4] showed an anti-correlation between undulation intensity and lipid area, indicating that increased undulations would compress the lipid area even further.

To shed more light on this topic, we have performed an extensive series of simulations of glycerolmonoolein (GMO) bilayers. GMO was chosen as a model lipid because it is small compared to the phospholipids used in the other studies, implying fast dynamics and shorter relaxation times. Also, the GMO headgroup does not possess a strongly polarized charge distribution, allowing the use of relatively small cutoffs. These two effects allow the study of the mesoscopic behavior of a large number of systems in which the equilibrium area, the surface tension, and system size are varied in a systematic way.

The overview of the remainder of this paper is as follows. In the next section we briefly summarize the theoretical background relating fluctuations in bilayer area, thickness, or undulations to macroscopic quantities such as bending constants and compressibilities. Then the simulation methodology and analysis is described, followed by the presentation of the results. Finally, we discuss the main implications of the results and summarize the conclusions.

## II. Theory

For length scales larger than the average thickness of the membrane $h_0$ the intensity of the undulatory modes with amplitude $u_{und}(q)$ as a function of the wave vector $q$ are predicted by a continuum model[9] to follow:

$$\langle u_{und}{}^2(q)\rangle = \frac{kT}{A(k_c q^4 + \gamma q^2)} \qquad q < q_0 \tag{1}$$

where $k_c$ denotes the bending modulus, $\gamma$ is the surface tension, $A$ is the system area, $k$ is Boltzmann's constant, $T$ is the temperature, and $q_0 = 2\pi/h_0$. Note that eq 1 assumes the absence of a spontaneous curvature, which should be zero for a symmetric bilayer. On smaller length scales the continuum picture is no longer valid. The undulatory modes will be dominated by collective or individual lipid protrusions. These modes can be described[10] by introducing a microscopic surface tension $\gamma_p$:

$$\langle u_{und}{}^2(q)\rangle = \frac{kT}{A\gamma_p q^2} \qquad q > q_0 \tag{2}$$

* Corresponding author. E-mail: marrink@chem.rug.nl. Fax: 31503634800.

10.1021/jp0103474 CCC: $20.00 © 2001 American Chemical Society
Published on Web 06/08/2001

Note that this microscopic surface tension is different from the macroscopic surface tension and only applies to length scales of a few lipid diameters at most.

Similarly, one can derive two regimes for the peristaltic membrane modes.[4] In the limit of long length scales the intensity of peristaltic modes with amplitude $u_{per} = (h - h_0)/2$ is given by

$$\langle u_{per}^2(q)\rangle = \frac{kT}{A(k_d q^4 + \gamma q^2 + k_e)} \qquad q < q_0 \tag{3}$$

where $k_d$ denotes the bending modulus for peristaltic modes (which is not necessary equal to $k_c$ as the monolayers bend anticorrelated rather than in a correlated way) and $k_e$ is a harmonic constant that was introduced to describe the force restoring the membrane thickness $h$ to its equilibrium value $h_0$. Again, on small length scales protrusion modes become dominant. Assuming that the monolayers at these small length scales behave independently, we have

$$\langle u_{per}^2(q)\rangle = \frac{kT}{A\gamma_p q^2} \qquad q > q_0 \tag{4}$$

similar to eq 2.

The peristaltic mode with $q = 0$ forms a special case. It equals $\delta h$; i.e., it measures the fluctuations in average bilayer thickness $(\langle h\rangle_z - h_0)/2$. Assuming that the volume compressibility of the membrane is much smaller than the area compressibility, we have

$$\langle u_{per}^2(0)\rangle = \frac{h_0^2}{4A^2}\langle \delta A_{per}\rangle^2 \tag{5}$$

where $\delta A_{per}$ is the amplitude of the area fluctuation due to peristaltic modes. The factor of 4 enters due to the definition of peristaltic amplitude as half the deviation from the mean bilayer thickness.

Ensemble theory[11] predicts for the general area fluctuations (both due to peristaltic and undulatory modes)

$$\langle \delta A\rangle^2 = \frac{kTA}{K_A} \tag{6}$$

with $K_A$ denoting the area compressibility modulus, which is also given by

$$K_A = A_0 \frac{\partial \gamma}{\partial A} \tag{7}$$

where $A_0$ is the equilibrium area. Assuming that peristaltic and undulatory modes occur in parallel and are independent of each other, their amplitudes should combine as

$$\langle \delta A\rangle^2 = \langle \delta A_{per}\rangle^2 + \langle \delta A_{und}\rangle^2 \tag{8}$$

$K_A$ can also be split into a peristaltic and an undulation part:

$$1/K_A = 1/K_A^{per} + 1/K_A^{und} \tag{9}$$

Combining the above equations allows us to relate $\langle u_{per}^2(0)\rangle$ to $K_A^{per}$:

$$K_A^{per} = \frac{h_0^2 kT}{4A\langle u_{per}^2(0)\rangle} \tag{10}$$

From solid mechanics models of thin films,[12] the undulatory part of the area compressibility modulus can be related to the bending modulus via

$$K_A^{und} = 48k_c/h_0^2 \tag{11}$$

## III. Method

**A. Simulation Details.** The standard GROMACS force field (v2.0)[13] was used to model the GMO molecules. The force field for GMO is similar to the one used by Wilson and Pohorille[14] in their simulation of a GMO bilayer. The partial charge distribution on the GMO headgroup was taken from their published values. All atoms were modeled explicitly, except for the hydrogens on the tail methyl groups, for which a united atom model was employed. All bond lengths and all angles involving the headgroup hydrogens were constrained using the LINCS algorithm.[15] The SPC model was used for the water molecules.[16] Its geometry was constrained with the SETTLE[17] algorithm. Because of the stability of the contraining algorithms, the use of a 5 fs time step was permitted.[18] A group based twin cutoff scheme was employed for the nonbonded interactions, with $R_{cut} = 1.0$ nm for Lennard-Jones and $R_{cut} = 1.2$ nm for electrostatic interactions. The absence of long range electrostatic interactions (the partial charges on the GMO headgroup are small, and there are no large dipolar interactions) allowed the use of this relatively short cutoff for the electrostatic interactions. In all directions periodic boundary conditions were applied. The system was coupled to a heat bath of 300 K and to a constant normal pressure of 1 atm (for fixed area simulations) or constant surface tension (for simulations at fixed surface tension) using standard weak coupling schemes.[19] Although pressure coupling using the Berendsen algorithm does not strictly produce a well-defined ensemble, test simulations involving lipid bilayers using Parrinello−Rahman and Nose−Hoover coupling schemes have not resulted in any noticeable effect on the observed fluctuations for correlation times larger than the coupling time (0.5 ps). As we are interested in the long time fluctuations only, we assume that our ensemble is representative of an isobaric ensemble.

An overview of the simulations that have been performed is given in Table 1. All systems contain a multiple of 50 GMO molecules, at a water/GMO ratio of 15. The swelling limit of GMO multilamellar systems is actually less,[20] but in the simulation box the system remains in a stable bilayer conformation. Including less water would suppress the magnitude of the undulations. Most simulations were performed at constant surface area, covering a range of area/lipid from 0.24 to 0.42 nm$^2$. A series of simulations was also performed at zero surface tension, and one simulation was performed at an increased surface tension in order to test whether ensembles generated from fixed area simulations and fixed surface tension simulations are comparable. The size of the system was varied from patches of 200 GMO molecules to patches of 1800 GMO molecules, covering a length range up to 15 nm. This length range was further extended to 20 nm by simulating rectangular patches with the $x$-dimension much larger than the $y$-dimension. To verify that this procedure does not lead to unwanted artifacts, we also simulated a smaller extended patch, which could be compared directly to a normal square patch. The measured surface tension and the magnitude of the undulations were very similar.

The generation of all the starting structures was as follows. First, a bilayer patch of 50 GMO molecules was constructed using an idealized all-trans configuration of a GMO molecule, at a surface area of 0.42 nm$^2$ per lipid. This system was solvated,

**TABLE 1: Overview of MD Simulations**

| label | no. of GMO | $L_{lat}$ (nm)[a] | $A_{lip}$ (nm$^2$) | time (ns) total − [eq] |
|---|---|---|---|---|
| Constant Surface Area Simulations ($NAP_zT$) | | | | |
| SQ200-A24 | 200 | 4.900 | 0.240 | 10 [1] |
| SQ200-A25 | 200 | 5.000 | 0.250 | 10 [1] |
| SQ200-A26 | 200 | 5.090 | 0.259 | 10 [1] |
| SQ200-A28 | 200 | 5.274 | 0.278 | 5 [1] |
| SQ200-A33 | 200 | 5.777 | 0.334 | 5 [1] |
| SQ200-A38 | 200 | 6.160 | 0.379 | 10 [1] |
| SQ200-A42 | 200 | 6.512 | 0.424 | 5 [1] |
| SQ800-A24 | 800 | 9.800 | 0.240 | 15 [4] |
| SQ800-A25 | 800 | 10.00 | 0.250 | 15 [4] |
| SQ800-A26 | 800 | 10.18 | 0.259 | 15 [4] |
| SQ800-A38 | 800 | 12.32 | 0.379 | 5 [1] |
| SQ1800-A26 | 1800 | 15.27 | 0.259 | 15 [5] |
| EX4×50-A26 | 200 | 10.18 | 0.259 | 20 [5] |
| EX8×50-A24 | 400 | 19.59 | 0.240 | 30 [10] |
| EX8×50-A25 | 400 | 20.02 | 0.250 | 30 [10] |
| EX8×50-A26 | 400 | 20.36 | 0.259 | 25 [5] |

| label | no. of GMO | $\gamma$ (mN/m) | time (ns) total − [eq] |
|---|---|---|---|
| Constant Surface Tension Simulations ($N\gamma P_zT$): | | | |
| SQ200-$\gamma$0 | 200 | 0 | 10 [1] |
| SQ200-$\gamma$85 | 200 | 85 | 5 [1] |
| SQ800-$\gamma$0 | 800 | 0 | 15 [4] |
| SQ1800-$\gamma$0 | 1800 | 0 | 16 [8] |
| EX8×50-$\gamma$0 | 400 | 0 | 40 [10] |

[a] For the extended simulations the elongated dimension is given − the shorter dimension is 4 times (EX4) or 8 times (EX8) smaller.

**TABLE 2: Equilibrium Properties**

| label | $P_{lat}$ ($10^5$ N/m$^2$) | $L_z$ (nm) | $\gamma$ (mN/m) | $SD_\gamma$[b] | $SE_\gamma$ | $\tau$ (ns) |
|---|---|---|---|---|---|---|
| Constant Area Simulations ($NAP_zT$) | | | | | | |
| SQ200-A24 | 47 | 8.6 | −40 | 11 | 2 | 0.5 |
| SQ200-A25 | −2 | 8.3 | −2 | 7 | 1 | 0.5 |
| SQ200-A26 | −39 | 8.0 | 33 | 6 | 1 | 0.5 |
| SQ200-A28 | −60 | 7.5 | 46 | 5 | 1 | 0.3 |
| SQ200-A33 | −127 | 6.3 | 82 | 3 | 1 | 0.2 |
| SQ200-A38 | −158 | 5.5 | 89 | 3 | 1 | 0.2 |
| SQ200-A42 | −192 | 5.0 | 97 | 2 | 1 | 0.2 |
| SQ800-A24 | 40 | 8.6 | −25 | 7 | 2 | 2 |
| SQ800-A25 | −2 | 8.3 | 2 | 6 | 2 | 3 |
| SQ800-A26 | −22 | 8.0 | 20 | 5 | 2 | 3 |
| SQ800-A38 | −156 | 5.5 | 90 | 2 | 2 | 1 |
| SQ1800-A26 | −24 | 8.0 | 22 | 4 | 3 | 5 |
| EX4×50-A26 | −24 | 8.0 | 21 | 10 | 2 | 3 |
| EX8×50-A24 | 19 | 8.6 | −16 | 7 | 2 | 6 |
| EX8×50-A25 | −6 | 8.3 | 4 | 7 | 2 | 6 |
| EX8×50-A26 | −20 | 8.0 | 16 | 5 | 2 | 5 |

| label | $L_{lat}$ (nm)[a] | $L_z$ (nm) | $A_{lip}$ (nm$^2$) | $SD_\gamma$[b] | $SE_\gamma$ | $\tau$ (ns) |
|---|---|---|---|---|---|---|
| Constant Surface Tension Simulations ($N\gamma P_zT$) | | | | | | |
| SQ200-$\gamma$0 | 5.03 | 8.3 | 0.251 | 0.001 | 0.0004 | 1 |
| SQ200-$\gamma$85 | 5.97 | 5.9 | 0.356 | 0.003 | 0.001 | 0.5 |
| SQ800-$\gamma$0 | 10.07 | 8.3 | 0.249 | 0.001 | 0.0005 | 3 |
| SQ1800-$\gamma$0 | 14.97 | 8.3 | 0.249 | 0.002 | 0.001 | 6 |
| EX8×50-$\gamma$0 | 19.90 | 8.4 | 0.247 | 0.002 | 0.0005 | 6 |

[a] For the extended simulations the elongated dimension is given; the shorter dimension is 4 times (EX4) or 8 times (EX8) smaller. [b] Note: sd's are for blocksize of $t = 1$ ns in all cases.

energy minimized, and equilibrated at constant area for a period of 5 ns. Copying this system twice in both lateral dimensions created the system labeled "SQ200-A42". This system was simulated at zero surface tension for 10 ns, and subsequently at a negative surface tension of −40 mN/m for another 2 ns in order to generate systems with smaller surface areas. Snapshots of these trajectories at the desired surface areas were selected as starting points for the other simulations. Larger systems were created by again lateral copying of smaller systems. Similarly, extended systems were created by one-dimensional copying of the original equilibrated 50 GMO patch. Newly created systems were equilibrated for at least 1 ns. For systems larger than 10 nm we found that much longer equilibration times (up to 10 ns) were needed. As was also found by Lindahl and Edholm,[4] the long wavelength undulatory and peristaltic modes take a long time to develop. Depending on the observed correlation times, systems were subsequently simulated for periods ranging from 5 to 30 ns (see Table 1). These runs were used for the analysis. The largest simulations (∼130 000 atoms) were performed in parallel on a Silicon Graphics Power Challenge, achieving a rate of ∼240 CPU hours/ns using 4 nodes.

**B. Analysis Details.** The surface tension $\gamma$ of the simulated system was computed from the pressure tensor via

$$\gamma = L_z(P_n - \langle P_{lat}\rangle) \tag{12}$$

where $P_n$ denotes the component of the pressure tensor normal to the bilayer (i.e., in the $z$-direction) and $\langle P_{lat}\rangle$ the average of the tangential components (i.e., in $x$- and $y$-directions). $L_z$ is the length of the simulation box in the $z$-direction.

For the computation of the $q$-dependent undulatory and peristaltic amplitudes, systems were mapped onto a grid with a grid spacing of 0.5 nm. For each voxel we determined the dominant phase, comparing local densities of water and GMO. The local bilayer position was then determined by performing an average in the $z$-direction of the position of the voxels having GMO as its dominant phase. Likewise, the local bilayer thickness was obtained by summation of these voxels in the $z$-direction. The discretized 2-dimensional maps were subsequently Fourier transformed to yield the spectral amplitudes and to obtain the spectral intensities. Time averaging was performed on the level of the intensities. Employing different strategies for determining the phase boundary or using smaller grid spacing did not significantly change the results for small $q$ values. For large $q$ values the method is unreliable as the concept of the bilayer surface becomes ill defined.

To obtain an estimate of the error in the calculated surface tensions, lipid areas, and bilayer undulatory and peristaltic amplitudes, the total simulation was divided into $n$ blocks and subaverages were calculated. Given a measured quantity $X$, the error in the expectation value $\langle X\rangle$ becomes independent of the number of blocks for block sizes larger than the correlation time $\tau$. The correlation time will be determined by the slowest modes present in the simulations. These are the undulatory and peristaltic modes with the maximum possible wavelength. These modes produce fluctuations in area or surface tension with the same correlation time. The error estimates presented in this paper are based on this block averaging procedure. In the figures are plotted 90% confidence intervals rather than standard errors. Depending on the number of independent blocks the 90% confidence intervals are a factor of 1.7−2.0 greater, assuming a Student $t$ distribution.

## IV. Results

Table 2 summarizes the equilibrium areas, surface tensions, and correlation times obtained from all simulations. The analysis of the results has been split into three subsections: undulatory modes, peristaltic modes, and area compressibilities.

**A. Undulatory Modes.** As Lindahl and Edholm[4] showed, at system sizes significantly larger than a correlation length of the

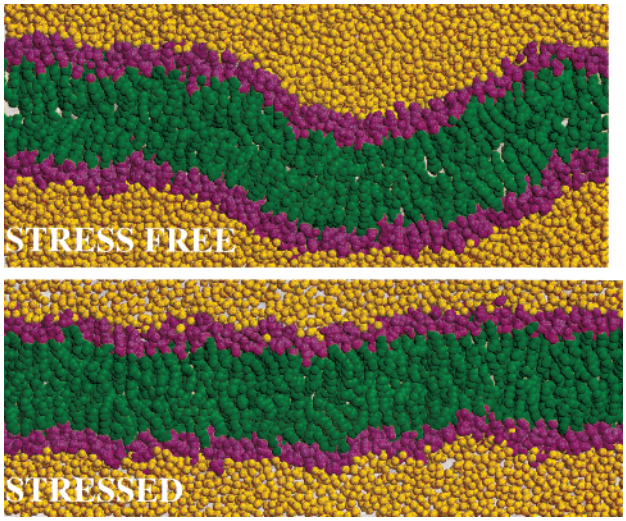


**Figure 1.** Two snapshots from extended simulations under stress free (upper) and stressed (lower) conditions, illustrating the appearance of long wavelength undulations in the first. Snapshots taken from simulations EX8×50-$\gamma$0 (upper) and EX8×50-A26 (lower). The GMO headgroups are colored purple, the tails green, and the water yellow. Note the reduced projected surface area when undulations are present.

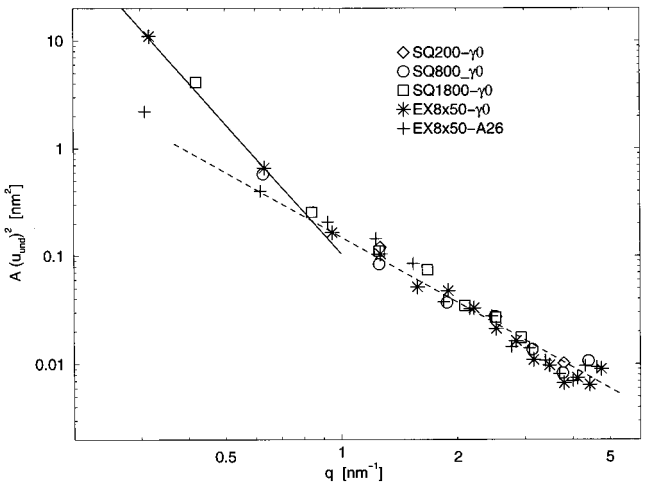


**Figure 2.** Spectral intensity for undulatory modes $u_{und}^2$ as a function of wavenumber $q$. Systems simulated at stress free conditions but differing in size are compared, plus one simulation at fixed area. The solid line indicates $q^4$ behavior observed for small $q$ values, the dashed line $q^2$ behavior observed for large $q$ values.

order of the thickness of the membrane, undulations appear. Figure 1 graphically shows the presence of long wavelength undulations for the system EX8×50-$\gamma$0, which was simulated at $\gamma = 0$, i.e., stress free conditions. It is compared to the system EX8×50-A26, which was simulated at a fixed area larger than the equilibrium area of the stress free membrane and therefore experienced a stress (of ∼16 mN/m) that clearly suppresses the undulations.

The results of the spectral analysis of the undulations are presented in Figure 2. We compare systems of different sizes at zero surface tension, plus one example of a system at stressed conditions. In general, one can see that the intensities, multiplied by the system area, do not depend on system size. Increasing the system size introduces new modes with longer wavelengths without changing the short wavelength modes. As expected from theoretical considerations, two scaling regimes can be observed. For small $q$ vectors the intensities are dominated by undulations and obey $q^4$ type scaling, whereas for large $q$ vectors the

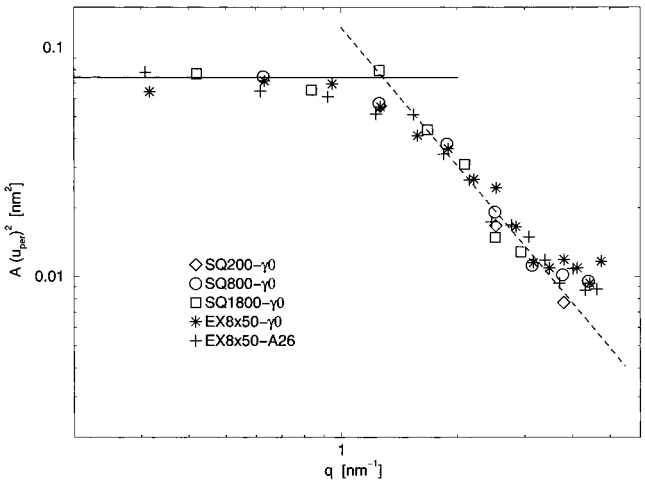


**Figure 3.** Spectral intensity for peristaltic modes $u_{per}^2$ as a function of wavenumber $q$. Systems simulated at stress free conditions but differing in size are compared, plus one simulation at fixed area. The solid line indicates limiting behavior for small $q$ vectors, the dashed line $q^2$ behavior observed for large $q$ values.

intensities are dominated by protrusion modes, following $q^2$ type scaling. Similar to the findings of Lindahl and Edholm,[4] the crossover occurs at a $q$ vector of approximately 1 nm$^{-1}$, which corresponds to a wavelength of ∼6 nm ($\simeq 2h_0$). Fitting of the results to eqs 1 and 2 gives $k_c = 4 \pm 2 \times 10^{-20}$ J and $\gamma_p = 17 \pm 4$ mN/m. The value of the bending constant is similar to the value of $k_c = 5 \times 10^{-20}$ J obtained by Lindahl[4] for a DPPC membrane. The microscopic surface tension is significantly smaller than their value of $\gamma_p = 50$ mN/m. Apparently, it is easier for the single tail surfactant GMO, than for the double tail lipid DPPC, to protrude out of the surface, thereby increasing the microscopic roughness. Comparison of the results for the stressed system EX8×50-A26 to the tensionless system EX8×50-$\gamma$0 clearly shows the suppression of the undulation modes due to the presence of a macroscopic surface tension. As the macroscopic surface tension for the stressed system is close to the microscopic one ($\gamma = 16 \pm 2$, $\gamma_p = 17 \pm 4$ mN/m), we observe virtually the same $q^2$ scaling over the whole range of $q$ vectors.

**B. Peristaltic Modes.** The spectral analysis of the peristaltic modes is presented in Figure 3. Unlike the undulatory modes, the amplitude of long wavelength modes is not diverging but instead reaches a maximum value, in accordance with the theoretical predictions (see eqs 3 and 4). For $q$ vectors smaller than the correlation length (which is ∼5 nm, somewhat smaller than observed for the undulatory modes) a protrusion dominated regime is found with $q^2$ scaling. Fitting of the results gives $k_e = (6 \pm 2) \times 10^{-20}$ J nm$^{-4}$ and $\gamma_p = 20 \pm 5$ mN/m. The value for the microscopic surface tension is the same (within error bars) as observed for the undulatory modes. The value of $k_e$ is about a factor of 10 larger than the value estimated by Lindahl and Edholm[4] for a DPPC membrane, indicating that the monolayer−monolayer restoring force is larger in the case of GMO. Another clear difference to the results obtained for DPPC is the absence of a regime dominated by peristaltic bending modes. Because of the smaller microscopic surface tension and the larger monolayer−monolayer restoring force observed for GMO with respect to DPPC, it is likely that the $q^4$ regime is effectively absent. As a consequence, the peristaltic intensities observed in our fixed area simulations are similar to those observed at zero surface tension, over the whole range of $q$ values except for $q = 0$. In the stress free simulations we find

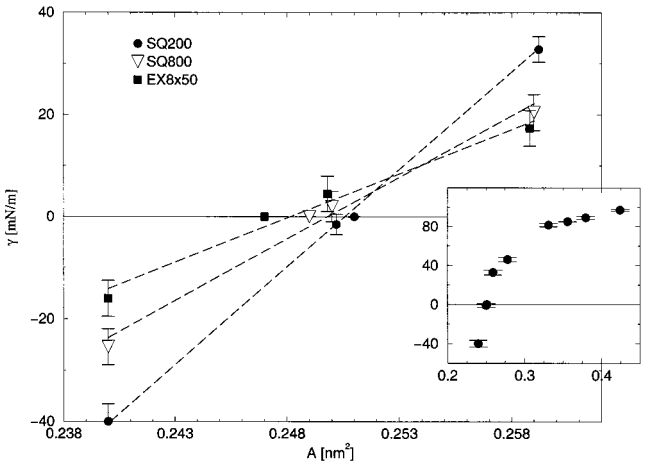


**Figure 4.** Dependence of surface tension $\gamma$ on area per lipid $A_{\mathrm{lip}}$. Systems of different sizes are compared. The dashed lines are linear fits of the data at a particular system size. The inset shows the extended scaling behavior for the SQ200 system. Error bars display 90% confidence intervals. Some data points are slightly shifted along the horizontal axis for clarity. See Table 2 for the exact numbers and for results not shown in this figure.

a $q = 0$ mode with a nonzero intensity, albeit much smaller compared to the intensities at low $q$. In the next subsection we relate this mode to the area compressibility of the system. The $q = 0$ mode intensity for the fixed area simulations vanishes, as it is coupled to the area fluctuations that are obviously suppressed in constant area simulations.

**C. Area Compressibility.** In Figure 4 is displayed the dependence of the macroscopic surface tension $\gamma$ on $A_{\mathrm{lip}}$, the area per lipid. The inset shows the dependence of $\gamma$ over an extended range of lipid area for the SQ200 simulations. It shows a steep surface tension dependence around the stress free area, leveling off toward larger areas. A similar qualitative picture was obtained for the simplified membranes studied by Goetz and Lipowsky.[12] The experimental surface area per lipid for GMO bilayers is estimated to be $\sim$0.34 nm$^2$ (diffraction[20]) and $\sim$0.38 nm$^2$ (black lipid[21]). Although the experimental determination of membrane surface area's is difficult, according to our data they correspond to a stressed state of the membrane. As GMO bilayers do not swell very much, it is not unreasonable to assume that indeed the experimental estimates are applicable to stressed membranes rather than freely undulating ones.

The main graph is focused around the equilibrium area under stress free conditions. Three different system sizes are compared: SQ200, SQ800, and EX8$\times$50. For all of the system sizes we observe linear behavior around the equilibrium area under stress free conditions. This is in agreement with the theoretical prediction of eq 7. From the slope of the curves we can obtain the area compressibility modulus, $K_A$. We find $K_A = 950 \pm 100$ mN/m, $K_A = 600 \pm 100$ mN/m, and $K_A = 430 \pm 100$ mN/m for the systems SQ200, SQ800, and EX8$\times$50, respectively. There is a clear size dependence in these numbers; the area compressibility modulus gets smaller as the system size increases. Larger systems are thus more easily compressible. This is a direct consequence of the appearance of undulation modes (see Figure 2) in larger systems. Excitation of long wavelength undulations is directly coupled to area compression. This is also evident from the system size dependence of the equilibrium area under stress free conditions. As long wavelength undulations appear, the projected surface area becomes smaller (see also Figure 1). The decrease in area is in apparent contrast to the findings of Lindahl and Edholm,[4] who observed the opposite effect for their DPPC membrane. Given that, even at length scales of $\sim$20 nm, the projected area is only marginally smaller than the unprojected local area, the effect only becomes apparent in long simulations of large systems. For systems that are small, of the order of a few lipid$-$lipid spacings only, the effect of periodic boundary conditions becomes important. Periodicity induces more order into the system and thereby reducing the area per lipid. An additional simulation at zero surface tension of our smallest building block consisting of only 50 GMO molecules displays such an effect. Its equilibrium area drops to 0.248 nm$^2$, smaller than that of the larger systems.

The area compressibility modulus can also be evaluated directly from the fluctuations in area of systems simulated at zero surface tension, using eq 6. Using this approach, we obtain $K_A = 930 \pm 60$ mN/m, $K_A = 680 \pm 60$ mN/m, $K_A = 650 \pm 120$ mN/m, and $K_A = 400 \pm 80$ mN/m for the systems SQ200, SQ800, SQ1800, and EX8$\times$50, respectively. These results are in good agreement with the values obtained above that were based on eq 7. Another method based on the local area fluctuations per lipid, used by Feller and Pastor[7] to obtain the area compressibility modulus of a DPPC membrane, should be considered with care. Fluctuations evaluated locally are much larger as they will reflect all the nonzero $q$ vector peristaltic modes. These, however, do not contribute to the macroscopic area fluctuations that determine the compressibility. This could explain the lower compressibilities these authors observe using this method.

It is possible to split the compressibility into an intrinsic part and an undulatory part, according to eq 9. The intrinsic part can be related to the $q = 0$ peristaltic mode intensity via eq 10. Using this equation, however, we obtain values for $K_A^{\mathrm{per}}$ that are very similar to the values quoted above for the total compressibility based on the total area fluctuations. It appears that the bilayer area fluctuations and the average bilayer thickness fluctuations (which is the $q = 0$ peristaltic mode) are strongly coupled, even for the larger systems that have entered the regime of strong undulatory excitations. This appears to be an artifact of the method of analysis. The bilayer thickness is measured by assuming that the bilayer is aligned in the *xy* plane. With the appearance of stronger undulations this approximation is no longer valid. For a proper evaluation of the bilayer thickness, one would have to define the orientation of the bilayer locally. Assuming that for our smallest system, SQ200, the area compressibility is almost entirely due to peristaltic modes, we estimate $K_A^{\mathrm{per}} \simeq 1000$ mN/m. On the basis of this value for $K_A^{\mathrm{per}}$ the contribution of undulatory modes to the overall area compressibility is estimated from eq 9 to be $K_A^{\mathrm{und}} \simeq 2000$ mN/m for the SQ800 system, and $K_A^{\mathrm{und}} \simeq 500$ mN/m for the EX8$\times$50 system. For length scales larger than $\sim$10 nm the contribution of undulatory modes thus becomes dominant. Comparing this value to the value of $K_A^{\mathrm{und}} \simeq 150$ mN/m obtained from the mean field prediction (eq 11), and using our earlier estimate of the bending rigidity constant $k_c$, it appears that either the mean field prediction is, at least quantitatively, not accurate or that it applies to even longer length scales.

## V. Discussion

As was previously found by Goetz and Lipowsky[12] for model lipid bilayers, and by Lindahl and Edholm[4] for realistic DPPC membranes, we observe a crossover between a length scale dominated by peristaltic and protrusion modes toward a length scale dominated by undulations. The intensity of these modes can be well described by a continuum model. The crossover occurs at a length scale that is almost twice as large as the

membrane thickness, at least in the case of stress free bilayers. Bilayers simulated at enlarged areas experience a stress or surface tension that suppresses very clearly the long wavelength undulations, even for system sizes much larger than the correlation length. Contrary to the observations by Tieleman and Berendsen[8] and in agreement with the observations by Feller and Pastor,[5] there is a strong dependence of the surface tension on surface area. Especially around the stress free equilibrium area the dependence is very steep (see Figure 4). As was noticed by Feller and Pastor,[7] the absence of this effect in the simulations of Tieleman and Berendsen[8] is likely to be due to their short sampling times (∼250 ps).

Long simulation times are indeed necessary to be able to distinguish differences in surface tensions or equilibrium areas. For the smallest systems simulated (200 surfactants) we find correlation times on the order of 0.5 ns, with fluctuations that are generally larger than the differences we are looking for (see Table 2). The situation is even more dramatic for larger systems. Long wavelength undulations show correlation times of more than 5 ns. Similarly, long correlation times were found for a DPPC bilayer by Lindahl and Edholm.[4] On the basis of these data, one should be careful when interpreting simulations of bilayers that do not sample at least a few multiples of these correlations times.

Looking at the system size dependence of the surface tension, it appears from Figure 4 that, for bilayers under stressed conditions (large area), the surface tension drops when the system size increases. This is the same effect as was originally observed by Feller and Pastor[5] in their simulation of DPPC bilayers, and which led them to the conclusion that a finite surface tension needs to be applied in small scale simulations to compensate for suppressed undulations. They tacitly assumed, however, that a similar drop in surface tension appears over the whole range of surface areas, including the stress free regime. In other words, they assumed that the area compressibility was independent of system size. If this were the case, the straight line fits in Figure 4 would run parallel. This is clearly not the case. We observe instead a crossing of these lines at a surface tension close to zero. Therefore, at stress free simulation conditions, the equilibrium area does not show a strong dependence on system size. The simulations of Lindahl and Edholm,[4] also at stress free conditions, show a similar behavior. This is contrary to the effect anticipated by Feller and Pastor,[5] i.e., that a small system simulated at stress free conditions produces an area much smaller than the equilibrium area of a much larger patch. In fact, the opposite effect is observed: a slightly smaller system area for the largest system simulated. This can be explained by the difference between the local area and the projected area of a bilayer that undergoes undulations. As the undulations become larger, the projected area will become smaller, assuming the local bilayer area remains unchanged. As a consequence, at surface areas slightly above the local equilibrium area the surface tension actually increases upon system enlargment.

On the basis of our current data plus that available from the literature (neglecting short simulations), we conclude that the application of an external surface tension to compensate for suppressed fluctuations is unnecessary, unless one wishes to reproduce experimental data that apply to bilayers actually under some sort of thermodynamic stress.

## VI. Conclusion

In agreement with simulation data of simplified lipid bilayers as well as DPPC bilayers, we have shown for GMO bilayers a crossover from a peristaltic and protrusion dominated regime to an undulatory regime for patches around twice the size of the bilayer thickness. As a result of the accessible undulatory modes, we observe a clear decrease in surface compressibility. This is an important effect having the consequence that whereas for stressed systems the surface tension drops upon system enlargment, under stress free conditions these changes are marginal. Because of a difference in projected and local lipid surface area the effect close to the stress free conditions is in fact reversed. Application of an external surface tension in MD simulations of bilayers to reproduce experimental surface areas for stress free systems is therefore unnecessary.

**Acknowledgment.** We thank Olle Edholm and Erik Lindahl for helpful discussions. S.J.M. is supported by the Royal Dutch Academy of Science (KNAW).

## References and Notes

(1) Tieleman, D. P.; Marrink, S. J.; Berendsen, H. J. C. *Biochim. Biophys. Acta* **1997**, *1331*, 235.

(2) Forrest, L. R.; Sansom, M. S. P. *Curr. Opin. Struct. Biol.* **2000**, *10*, 174.

(3) Feller, S. *Curr. Opin. Colloid Interface Sc.* **2000**, *5*, 218.

(4) Lindahl, E.; Edholm, O. *Biophys. J.* **2000**, *79*, 426.

(5) Feller, S. E.; Pastor, R. W. *Biophys. J.* **1996**, *71*, 1350.

(6) Jähnig, F. *Biophys. J.* **1996**, *71*, 1348.

(7) Feller, S. E.; Pastor, R. W. *J. Chem. Phys.* **1999**, *111*, 1281.

(8) Tieleman, D. P.; Berendsen, H. J. C. *J. Chem. Phys.* **1996**, *105*, 4871.

(9) Safran, S. A. *Statistical Thermodynamics of Surfaces, Interfaces, and Membranes*; Addison-Wesley: Reading, MA, 1994.

(10) Lipowsky, R.; Grotehans, S. *Europhys. Lett.* **1993**, *23*, 599.

(11) Allen, M. P.; Tildesley, D. J. *Computer Simulation of Liquids*; Clarendon Press: Oxford, 1987.

(12) Goetz, R.; Lipowsky, R. *J. Chem. Phys.* **1998**, *108*, 7397.

(13) Van Der Spoel, D.; Van Buuren, A. R.; Apol, E.; Meulenhoff, P. J.; Tieleman, D. P.; Sijbers, A. L. T. M.; Van Drunen, R.; Berendsen, H. J. C. *Gromacs User Manual version 1.2*, Nijenborgh 4, 9747 AG Groningen, The Netherlands. Internet: http://rugmd0.chem.rug.nl/gmx, 1996.

(14) Wilson, M. A.; Pohorille, A. *J. Am. Chem. Soc.* **1994**, *116*, 1490.

(15) Hess, B.; Bekker, H.; Berendsen, H. J. C.; Fraaije, J. G. E. M. *J. Comput. Chem.* **1997**, *18*, 1463.

(16) Berendsen, H. J. C.; Postma, J. P. M.; Gunsteren, W. F.; Hermans, J. Interaction models for water in relation to protein hydration. In *Intermolecular Forces*; Pullman, B., Ed.; Reidel: Dordrecht, The Netherlands, 1981; pp 331−342.

(17) Miyamoto, S.; Kollman, P. A. *J. Comput. Chem.* **1992**, *13*, 952.

(18) Feenstra, K. A.; Hess, B.; Berendsen, H. J. C. *J. Comput. Chem.* **1999**, *20*, 786.

(19) Berendsen, H. J. C.; Postma, J. P. M.; Van Gunsteren, W. F.; Dinola, A.; Haak, J. R. *J. Chem. Phys.* **1984**, *81*, 3684.

(20) Briggs, H. C. J.; Caffrey, M. *J. Phys. II Fr.* **1996**, *6*, 723.

(21) White, S. H. *Biophys. J.* **1978**, *23*, 337.